11th World Congress on Computational Mechanics (WCCM XI)
5th European Conference on Computational Mechanics (ECCM V)
6th European Conference on Computational Fluid Dynamics (ECFD VI)
E. Oñate, J. Oliver and A. Huerta (Eds)

MICROMECHANICAL FAILURE MODELLING OF COMPOSITE MATERIALS USING HFGMC

DARKO IVANČEVIĆ AND IVICA SMOJVER

University of Zagreb, Faculty of Mechanical Engineering and Naval Architecture
I. Lučića 5, 10000 Zagreb, Croatia
e-mail: divancevic@fsb.hr, ismojver@fsb.hr, http://aerodamagelab.fsb.hr

Key Words: *Micromechanics, damage modelling, multiscale analysis, composite structures.*

Abstract. In order to improve the failure analysis of complex composite structures, a two-scale damage prediction procedure has been developed. The methodology is based on the High Fidelity Generalized Method of Cells (HFGMC) model which belongs to a group of computationally efficient semi-analytical micromechanical models. The methodology has been developed with the aim of modelling high velocity impact damage on aeronautical structures using Abaqus/Explicit to perform computations at the structural level. The link between the finite element macro-level analysis and the micromechanical model has been achieved with the user material subroutine VUMAT, which for each material point performs micromechanical calculations based on the applied macroscopic strain given by the FE analysis. As a result, failure processes of complex composite structures have been modelled using micromechanical principles. Several constituent based failure initiation criteria have been implemented in the methodology. A complex multiaxial damage model has been included in the calculations. The results of the micromechanical damage model agree well with ply-based calculation of the Puck failure model. The procedure has been tested on a numerical example in which a soft-body impactor impacts a GFRP plate.

1 INTRODUCTION

Failure modes of composite materials are a result of the material heterogeneous microstructure. Consequently, failure of composite materials is manifested as a fibre breakage, matrix failure, fibre pullout, delamination or as a combination of these failure modes. The conventional approach in design and seizing of composite structures is the application of failure criteria at the level of a homogenized composite ply. The accuracy of numerical failure predictions can be increased by modelling of damage processes at the micro-structural level of the heterogeneous material. In order to enable application of micromechanical design methods on engineering problems, a two-scale approach has to be employed.

The presented work is a continuation of previous research in which a numerical damage modelling procedure has been developed focusing on the soft-body impact analysis of aeronautical composite structures [1, 2]. The methodology has been extended by application of a two-scale procedure in modelling of composite materials. The HFGMC micromechanical model [3] has been employed for analyses on the micromechanical level, while Abaqus/Explicit has been used for the solution of the macromechanical problem.

The micromechanical damage modelling procedure has been applied on a high velocity impact problem in this work. The methodology has been based on the computationally efficient HFGMC models [4], since explicit FE analyses solve dynamic nonlinear problems using a large number of very small time increments. Micromechanical modelling is particularly suitable for nonlinear phenomena in composite materials – e.g. damage effects and viscoplasticity caused by high strain rates. In these nonlinear problems, the constitutive responses of the fibre and matrix show significant differences. The resulting effect of the diverse mechanical responses of the constituents on the equivalent composite mechanical properties cannot be predicted accurately using homogenised theories.

2 MICROMECHANICAL MODEL

The HFGMC model belongs to a wide range of micromechanical models developed from the Method of Cells (MOC) [5]. Since the complete HFGMC theory is very complex, only the most important relations are summarized in this work. An important feature of micromechanical models is the Repeating Unit Cell (RUC) concept. The unit cell is a basic building element which characterizes the evaluated heterogeneous material. The RUC concept assumes a perfectly periodic pattern of the unit cells in the material. A common feature of all MOC-based micromechanical models is the discretization of the unit cell using $N_\beta \times N_\gamma$ subcells. Figure 1 shows basic variables and discretization scheme of the HFGMC model. The right-hand side image on Figure 1 shows an example of a 30 x 30 HFGMC model for a composite material with 60% fibre volume fraction. The two-dimensional HFGMC model is applicable for unidirectional fibre-reinforced materials. Fibres, which extend in the x_1-direction, are arranged in a doubly periodic array in the x_2 and x_3 directions. The coordinate system used for the micromechanical model corresponds to the principal material coordinate system of the composite ply, as x_1 is aligned with the fibre direction, x_2 lies in the ply plane and x_3 is perpendicular to the ply plane.

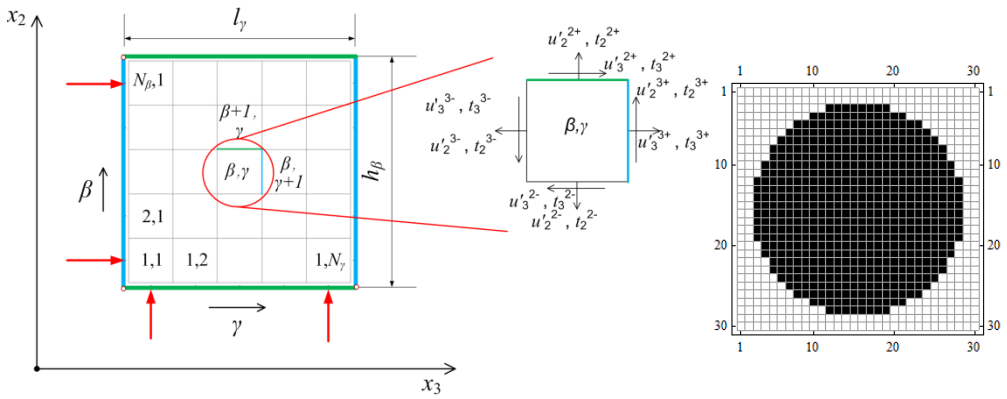

Figure 1: HFGMC model with displacement and traction components (left-hand side image) and example of 30x30 RUC for a composite with 60% fibre volume fraction

The constitutive response of each subcell is governed by the elasticity tensor $\mathbf{C}^{(\beta,\gamma)}$ of the β,γ subcell. Consequently, the number of material phases or constituents is limited only by

the number of subcells. Periodic boundary conditions are imposed on the boundaries of the RUC, whereas traction and displacement continuity conditions are applied at subcell boundaries within the RUC. Additionally, four displacement components are constrained in order to prevent unit cell rigid body motion as displayed by the four arrows at the unit cell borders in Figure 1. The aim of the micromechanical models is to determine the homogenized mechanical properties of the composite material. An additional capability of more advanced micromechanical models is prediction of the stress and strain fields within the unit cell of the composite material. For MOC-based micromechanical models, the strain field within the unit cell is calculated as

$$\overline{\boldsymbol{\varepsilon}}^{(\beta,\gamma)} = \mathbf{A}^{(\beta,\gamma)}\overline{\boldsymbol{\varepsilon}}\,, \tag{1}$$

where $\overline{\boldsymbol{\varepsilon}}^{(\beta,\gamma)}$ is the strain tensor of the β,γ subcell, while $\overline{\boldsymbol{\varepsilon}}$ is the homogenized strain state. $\mathbf{A}^{(\beta,\gamma)}$ is the strain concentration tensor of the β,γ subcell which enables solution of the micromechanical problem. The homogenized mechanical properties of the composite material are determined using the relation

$$\mathbf{C}^{*} = \frac{1}{hl}\sum_{\gamma=1}^{N_\gamma}\sum_{\beta=1}^{N_\beta} h_\beta l_\gamma \mathbf{C}^{(\beta,\gamma)}\mathbf{A}^{(\beta,\gamma)}, \tag{2}$$

where h_β and l_γ are subcell dimensions as shown in Figure 1.

The reformulated HFGMC model with enhanced computational efficiency [4] has been employed in this methodology. The model employs second order Legendre polynomials to approximate the displacement $u_i^{(\beta,\gamma)}$ field within the RUC, after

$$\begin{aligned} u_i^{(\beta,\gamma)} = \overline{\varepsilon}_{ij}x_j + W_{i(00)}^{(\beta,\gamma)} + \overline{y}_2^{(\beta)}W_{i(10)}^{(\beta,\gamma)} + \overline{y}_3^{(\gamma)}W_{i(01)}^{(\beta,\gamma)} + \frac{1}{2}\left(3\overline{y}_2^{(\beta)2} - \frac{h_\beta^2}{4}\right)W_{i(20)}^{(\beta,\gamma)} + \\ + \frac{1}{2}\left(3\overline{y}_3^{(\gamma)2} - \frac{l_\gamma^2}{4}\right)W_{i(02)}^{(\beta,\gamma)},\ \ i,j = 1,2,3. \end{aligned} \tag{3}$$

The *W* variables in Equation 3 are micromechanical variables which have to be calculated in order to determine the micromechanical displacement field. As opposed to the original HFGMC model, the reformulated model introduces a local-global stiffness matrix approach with significant computational advantages [6]. The global stiffness matrices of the unit cell are assembled after application of traction and continuity conditions at subcell interfaces and periodicity equations at unit cell boundaries, as explained in [4,6]. The global system of equations can be decoupled into axial (Equation 4) and transverse (Equation 5) sets of equations

$$\begin{bmatrix} \mathbf{L}_{11} & \mathbf{L}_{12} \\ \mathbf{L}_{21} & \mathbf{L}_{22} \end{bmatrix} \begin{Bmatrix} \begin{bmatrix} \overline{\mathbf{u}}_1'^2 \end{bmatrix} \\ \begin{bmatrix} \overline{\mathbf{u}}_1'^3 \end{bmatrix} \end{Bmatrix} = \begin{bmatrix} \boldsymbol{\Delta}\mathbf{c}_{11} & \mathbf{0} \\ \mathbf{0} & \boldsymbol{\Delta}\mathbf{c}_{22} \end{bmatrix} \begin{Bmatrix} \overline{\varepsilon}_{12} \\ \overline{\varepsilon}_{13} \end{Bmatrix}, \tag{4}$$

$$\begin{bmatrix} \mathbf{K}_{11} & \mathbf{0} & \mathbf{K}_{13} & \mathbf{K}_{14} \\ \mathbf{0} & \mathbf{K}_{22} & \mathbf{K}_{23} & \mathbf{K}_{24} \\ \mathbf{K}_{31} & \mathbf{K}_{32} & \mathbf{K}_{33} & \mathbf{0} \\ \mathbf{K}_{41} & \mathbf{K}_{42} & \mathbf{0} & \mathbf{K}_{44} \end{bmatrix} \begin{Bmatrix} \overline{\mathbf{u}}_2'^2 \\ \overline{\mathbf{u}}_3'^2 \\ \overline{\mathbf{u}}_2'^3 \\ \overline{\mathbf{u}}_3'^3 \end{Bmatrix} = \begin{bmatrix} \Delta\mathbf{C}_{11} & \Delta\mathbf{C}_{12} & \Delta\mathbf{C}_{13} & \mathbf{0} \\ \mathbf{0} & \mathbf{0} & \mathbf{0} & \Delta\mathbf{C}_{24} \\ \mathbf{0} & \mathbf{0} & \mathbf{0} & \Delta\mathbf{C}_{34} \\ \Delta\mathbf{C}_{41} & \Delta\mathbf{C}_{42} & \Delta\mathbf{C}_{43} & \mathbf{0} \end{bmatrix} \begin{Bmatrix} \overline{\varepsilon}_{11} \\ \overline{\varepsilon}_{22} \\ \overline{\varepsilon}_{33} \\ \overline{\varepsilon}_{23} \end{Bmatrix}. \tag{5}$$

Global **L** and **K** matrices are assembled from the subcell local stiffness matrices as explained in [6]. The submatrices $\Delta\mathbf{c}$ in the axial system and $\Delta\mathbf{C}$ in the transverse system of equations contain differences in elastic stiffness elements between adjacent subcells, after [6]. The solution of the global system of equations for the unknown fluctuating displacement components enables calculation of the microvariables *W* in Equation (3), which are used to calculate the unknown strain field $\overline{\boldsymbol{\varepsilon}}^{(\beta,\gamma)}$. The strain concentration tensors are obtained using a numerical procedure as explained in [4].

2.1 Micromechanical failure criteria and damage model

Constituent-based failure criteria are employed for modelling of damage initiation at the micromechanical level. Validation of several micromechanical failure models has been presented in [7]. The work in this paper focuses on the micromechanical damage model introduced in [8]. Only the most important relations of the damage model are provided in this work, while the complete overview of the theory is presented in [8]. The multiaxial continuum damage model is applied only for the matrix, whereas the failure initiation in fibre subcells results with complete subcell failure. This state is modelled by applying very low values to the subcell elasticity properties (0.0001 times the undamaged values). The maximal stress criterion has been used to predict failure in fibre subcells. The theory introduces damage strains defined as

$$\begin{aligned} \varepsilon_1^D &= \sqrt{\left(\frac{\varepsilon_{11}}{X_\varepsilon}\right)^2 + \left(\frac{\gamma_{13}}{R_\varepsilon}\right)^2 + \left(\frac{\gamma_{12}}{S_\varepsilon}\right)^2}, \\ \varepsilon_2^D &= \sqrt{\left(\frac{\varepsilon_{22}}{Y_\varepsilon}\right)^2 + \left(\frac{\gamma_{23}}{Q_\varepsilon}\right)^2 + \left(\frac{\gamma_{12}}{S_\varepsilon}\right)^2}, \\ \varepsilon_3^D &= \sqrt{\left(\frac{\varepsilon_{33}}{Z_\varepsilon}\right)^2 + \left(\frac{\gamma_{23}}{Q_\varepsilon}\right)^2 + \left(\frac{\gamma_{13}}{R_\varepsilon}\right)^2}, \end{aligned} \tag{6}$$

where X_ε, Y_ε and Z_ε variables denote the normal failure strains in the *1*, *2* and *3* material direction, as defined in Figure 1. These allowable strain values usually have different values in tensile and compressive loading modes, as shown in Table 1 for the MY750 epoxy matrix which has been used throughout this work. R_ε, Q_ε and S_ε variables in Equation 6 are failure engineering shear strains. Table 1 contains mechanical properties of the fibre and matrix as well as all necessary parameters of the matrix damage model [8]. The damage strains defined in Eq. 6 have the same function as the left-hand sides of commonly used failure criteria for fibre reinforced composite materials, indicating initiation of damage processes if their values

exceed 1.0.

Damage evolution in matrix material is tracked using three tensile and three compressive damage variables D_i. The incremental changes of damage variables and associated degradation of mechanical properties during a load increment are calculated using the relation

$$dD_i = (1 - D_i - k_i^{'}) \frac{d\varepsilon_i^D}{\varepsilon_i^D}, \tag{7}$$

where $d\varepsilon_i^D$ is the increment of the damage strain. The post-peak tangent modulus is modelled using the slope parameter $k_i^{'}$, calculated as

$$k_i^{'} = Ae^{-\varepsilon_i^D / B}, \tag{8}$$

with *A* and *B* as the post-damage slope parameters. The damage model separates degradation processes in tensile and compressive failure modes

$$\begin{aligned} D_i^T &= D_{i\ old}^T + dD_i \quad \text{for } \varepsilon_{ii} > 0, \\ D_i^C &= D_{i\ old}^C + dD_i \quad \text{for } \varepsilon_{ii} < 0. \end{aligned} \tag{9}$$

The elasticity properties of the damaged matrix subcell are degraded using

$$E_i = d_i E_i^0 \quad \text{for } i = 1,2,3, \tag{10}$$

$$\nu_{ij} = d_i \nu_{ij}^0 \quad \text{for } i, j = 1,2,3. \tag{11}$$

where the d_i variables are calculated as

$$d_i = \begin{cases} 1 - b_{ii}^T D_i^T & \text{for } \sigma_{ii} > 0 \\ 1 - b_{ii}^C D_i^C & \text{for } \sigma_{ii} < 0. \end{cases} \tag{12}$$

The *b* parameters in Equation 12 are the scaling parameters. The final failure of matrix subcells is predicted using damage energy principles. The strain energy density is calculated as

$$dW_i = \frac{1}{2}\left\{\sigma_i\left(\varepsilon_i + d\varepsilon_i\right) - \varepsilon_i\left(\sigma_i + d\sigma_i\right)\right\}. \tag{13}$$

The final failure criterion is associated with the loading modes - Mode I (opening), Mode II (in-plane shear) and Mode III (out of plane shear). The mode-specific strain energy release rates (SERR) are

$$\begin{aligned} G_I^1 &= \frac{l_1}{b_{11}^T}\frac{dW_I^1}{dD_1}, \quad G_{II}^1 = \frac{l_1}{b_{61}}\frac{dW_{II}^1}{dD_1}, \quad G_{III}^1 = \frac{l_1}{b_{51}}\frac{dW_{III}^1}{dD_1}, \\ G_I^2 &= \frac{l_2}{b_{22}^T}\frac{dW_I^2}{dD_2}, \quad G_{II}^2 = \frac{l_2}{b_{42}}\frac{dW_{II}^2}{dD_2}, \quad G_{III}^2 = \frac{l_2}{b_{62}}\frac{dW_{III}^2}{dD_2}, \\ G_I^3 &= \frac{l_3}{b_{33}^T}\frac{dW_I^3}{dD_3}, \quad G_{II}^3 = \frac{l_3}{b_{53}}\frac{dW_{II}^3}{dD_3}, \quad G_{III}^3 = \frac{l_3}{b_{43}}\frac{dW_{III}^3}{dD_3}, \end{aligned} \tag{15}$$

where b_{ij} denote scaling parameters, while l_i is the characteristic material length. The W_M^i variables in Equation 15 are mode specific strain energy density release rates, after [8]. Complete degradation of matrix subcells properties in tensile loading modes is determined if the mode-specific strain energy release rates reach the material critical strain release rate

$$G_M^i \geq G_M^C, \quad M = I, II, III. \tag{16}$$

Failure prediction in compressive loading modes has been predicted using the criterion

$$\left(W_I^i + W_{II}^i + W_{III}^i\right)V = W_S^C, \tag{17}$$

where V is the volume of the material and W_S^C is the critical compressive strain energy.

Table 1: Fibre and matrix mechanical properties and properties of the damage model [8]

Silenka E-glass fibre				
E [GPa]	ν[–]	X^T [MPa]	X^C [MPa]	
74	0.2	2110	1290	
MY750 epoxy matrix				
E [GPa]	ν[–]	X_ε^T[–]	X_ε^C[–]	S_ε[–]
3.7	0.35	0.0125	0.0287	0.0443
Post-damage slope parameters				
$A^T = 0.7$	$A^C = 2.0$	$B^T = 0.82$	$B^C = 0.96$	
Scaling parameters				
$b_{ii}^T = b_{ii}^C = 1.32$		$b_{4i} = b_{5i} = b_{6i} = 0.50$		
Critical energy release rates				
Property		Symbol	Value	
Mode I SERR		G_I^C	800 J/m^2	
Mode II and III SERR		$G_{II}^C = G_{III}^C$	2400 J/m^2	
Critical compressive strain energy		W_S^C	1.86×10^{-6} J	
Material length		l_i	9.0×10^{-5} m	

3 MULTISCALE FRAMEWORK

The Abaqus/Explicit user material subroutine VUMAT has been employed in the presented methodology as to enable implementation of the HFGMC model. Within the two-scale method, HFGMC has been programmed as a subroutine which is called from VUMAT at every material point of the FE model throughout the explicit analysis.

The aim of the HFGMC model is to predict the equivalent composite constitutive behaviour, given mechanical properties of the constituents and parameters which define the

RUC of the composite material – unit cell morphology, fibre volume fraction, number and location of fibre centres. The determination of strain concentration tensors enables calculation of the micromechanical strain and stress tensors within the heterogeneous material unit cell, as explained in Section 2. The HFGMC model has also been employed to model damage and degradation effects of the composite material at the micro-structural level. In order to enable micromechanical modelling of nonlinear constitutive models as e.g. plasticity and damage, an incremental-iterative procedure has been included in the micromechanical model. Implementation of the iterative-incremental procedure solves problems which occur by acceptance of the linearized trial solution of the micromechanical model. These errors would be generated by micromechanical strain field calculation using strain concentration tensors which have been determined with initial subcell elasticity properties, after [9]. The HFGMC and VUMAT coupling has been achieved using a total of 44 Solution Dependent state Variables (SDV) and 47 common blocks which are necessary to transfer variables of the micromechanical model in matrix form from the current to the following time increment in the explicit analysis.

4 RESULTS

4.1 Multiscale application

The described multiscale approach has been developed as an upgrade to the bird strike damage methodology presented in [1,2]. In order to demonstrate the multiscale damage procedure, a high velocity soft body impact has been simulated in which a numerical bird replacement impactor impacts a composite plate. Parameters of the numerical setup have been derived from the experimental high velocity gas-gun experiments, provided in [10]. Details of the numerical setup have been provided in [2], while the parameters of the model in this work have been adjusted as to employ the E-glass/epoxy micromechanical model with properties listed in Table 1.

The numerical model is shown in Figure 2. The impactor has been modelled by the Coupled Eulerian Lagrangian (CEL) formulation [11]. The CEL approach is a numerical technique employed in those analyses where large deformations of conventional (Lagrangian) finite elements could cause numerical difficulties. Within the CEL method, the soft-body impactor has been modelled as Eulerian material which flows through the static Eulerian finite element mesh, while the impacted plate has been modelled using Lagrangian shell elements. The general contact algorithm has been used to model the contact between the FE mesh of the composite plate and the impactor material.

Dimensions of the composite plate are 216 x 102 mm. The boundary conditions have been selected as to replicate the experimental setup in [10]. In these experiments, a 25 mm wide clamp has been applied to one of the shorter plate edges. This boundary condition has been simulated by the restriction of all degrees of freedom of the nodes in the clamped part of the composite plate, as shown in the right-hand side image in Figure 2. The plate geometry has been discretized using 860 conventional shell finite elements. The composite plate is 3 mm thick and consists of 21 CFRP E-glass/epoxy plies with a $[(0_2/\ 90_2)_2/0/90/\overline{0}]_S$ layup, where the layup reference angle has been measured with regard to the longer plate edge. The mechanical properties of the unidirectional plies have been predicted using the 30x30

HFGMC model in Figure 1 and the constituent properties provided in Table 1. The calculated homogenized properties are shown in Table 2.

Table 2: Homogenized composite properties calculated by HFGMC, Vf = 60%

$E_1[\text{GPa}]$	$E_2[\text{GPa}]$	$G_{12}[\text{GPa}]$	$\nu_{12}[-]$	$\nu_{23}[-]$
45.911	16.332	5.043	0.249	0.259

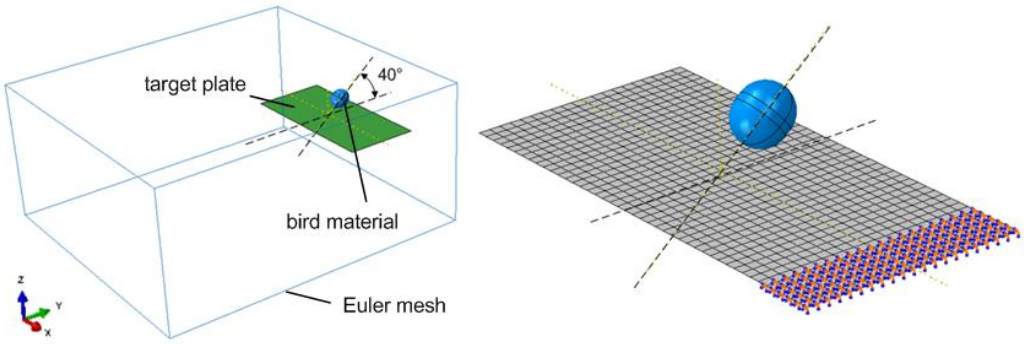

Figure 2: CEL numerical model

The size of the cube containing the Eulerian elements has to be sufficiently large to prevent the impactor material from escaping the Eulerian mesh. The dimensions of the cube are therefore 0.45 x 0.4 x 0.2 m, while the Eulerian mesh consists of 487,920 elements. The impactor has been defined in [10] as a body with a 25 mm diameter, mass of 10 g and material density of 1010 kg/m^3. As the exact shape of the impactor has not been specified, the conventional shape used in the numerical bird strike simulation has been employed in this work as well. Accordingly, the substitute bird geometry has been replaced by a cylinder with hemispherical ends. The impactor material model has been modelled using the Mie-Grüneisen Equation of State with properties similar to water, as explained in [1].

The initial velocity vector, with a magnitude of 100 m/s, is deflected by 40° with respect to the composite plate plane, as shown in Figure 2. The impact point is located at the centre of the unclamped part of the composite plate. The results provided in this work show the initial impact event for which a total time of 0.2 ms has been analyzed.

4.1 Results of the analysis

Figures 3 – 6 show results of the soft-body impact. The clamped end of the composite plate is located on the right side of the images in Figures 4 - 6. The impact event and bird material deformation is shown in Figure 4. The contours in Figure 4 visualize the displacements in the *z* direction, which is perpendicular to the composite plate as defined in Figure 2. The results demonstrate the ability of the numerical bird model to replicate the very high deformations of the soft-body impactor.

Results of the micromechanical failure model have been compared with results of the ply-based Puck's failure model, as this failure theory has showed very good results in the World Wide Failure Exercise (WWFE) [12]. The strength properties of the homogenized GFRP

plies, used to calculate Puck's ply-based failure criterion have been taken from [13], while the parameters of the Puck failure model have been defined in [14]. The results of the Puck's failure criteria have been used only to compare results of the micromechanical damage model, whereas progressive damage models have not been applied to this ply based failure model.

The SDV's associated with micromechanical failure criteria show the maximal value within the RUC associated to the relevant FE material point. The results in Fig. 4 show the maximal through thickness values of the criterion.

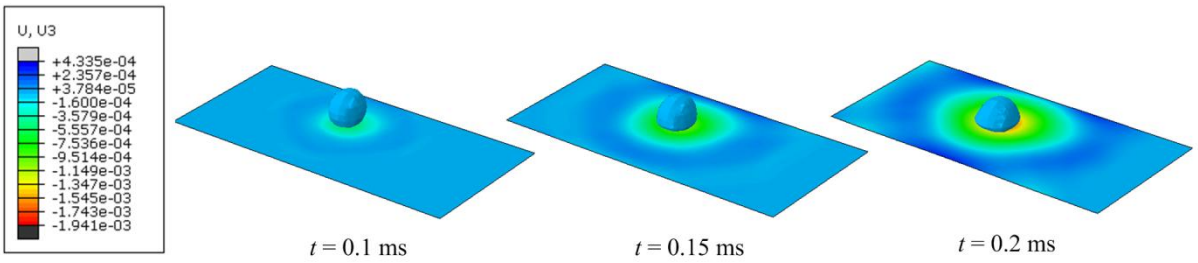

Figure 3: Visualization of the impact event. The contours show displacements in the direction perpendicular the composite plane [m]

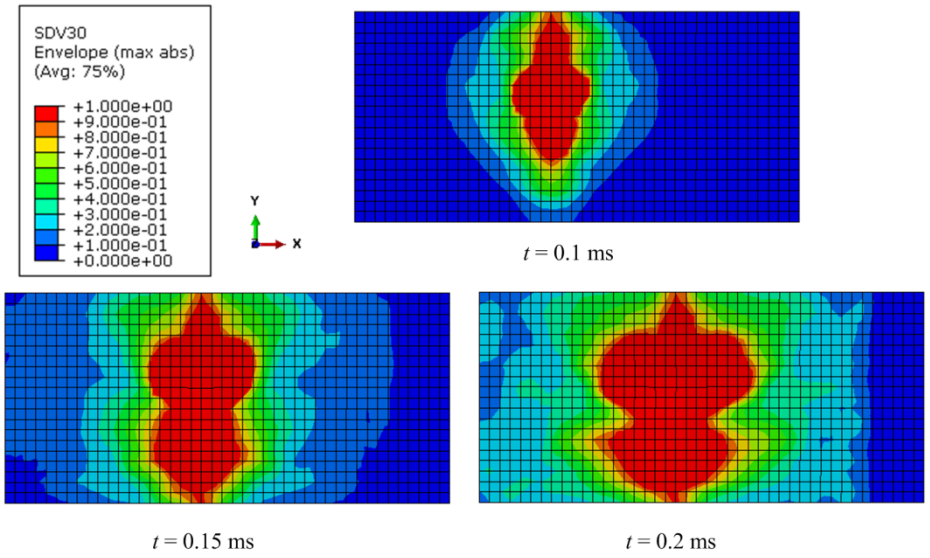

Figure 4: Visualization of the evolution of ε_2^D damage strain (maximal through thickness values are shown)

Figure 4 shows contours of the damage strain criterion for three time steps of the analyzed impact event. Results of the analysis show that ε_2^D damage strain reached the highest value of the three damage strains defined in Equation 6 and predicts degradation of mechanical properties in a very large part of the composite plate. ε_2^D is the primary mode of failure in this analysis, while ε_1^D and ε_3^D reach lower values.

Although the impact caused severe matrix damage, fibre failure has not been predicted to occur in the analysis. The maximum stress criterion has reached maximal values of 0.23. This

result agrees well with the Puck's ply-based fibre failure criteria which reaches maximal values of 0.26.

The results shown in Figures 5 and 6 refer to the composite plies oriented by 0° and located on the side of the composite plate opposite to the impact location. The damage effects are more pronounced on material points of this side of the composite plate due to lower failure initiation properties in the tensile loading regime, as shown in Table 1.

The effect of degradation on homogenized composite E_2 and G_{12} elasticity properties is shown in Figure 5. The initial values of E_2 and G_{12} have been degraded in the areas where the ε_2^D damage strains reach values above 1.

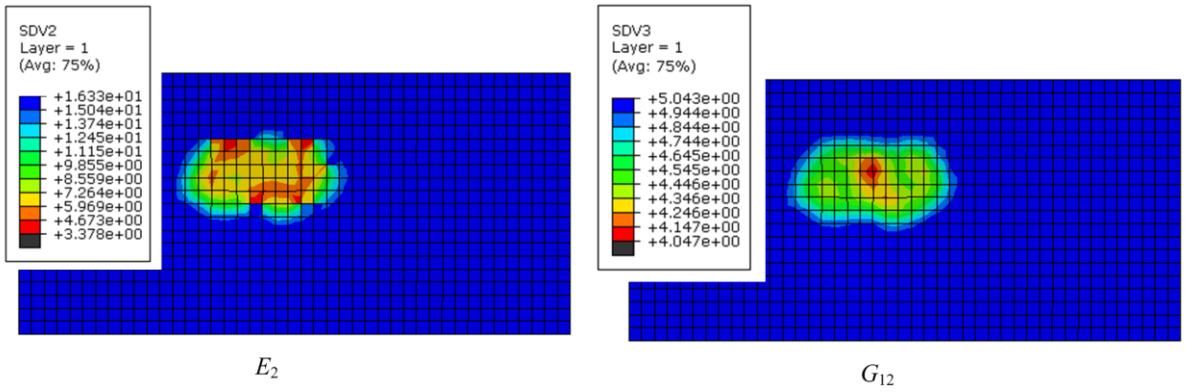

Figure 5: Degraded values of E_2 and G_{12} [GPa]

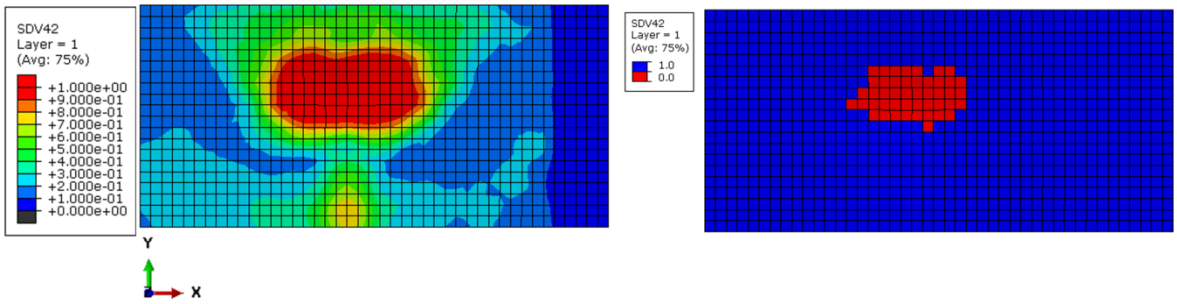

Figure 6: Comparison of Puck mode A failure criterion (left-hand side image) with the SDV controlling material point failure as predicted by the micromechanical model (right-hand side image)

Figure 6 shows a comparison of Puck's Mode A matrix failure criterion and the SDV controlling element deletion from VUMAT, calculated by the micromechanical model. In order to remove an element from the analysis, this SDV has to be set to zero in all material points of the element. Complete failure of a material point has in this analysis been determined if subcell failure occurs in at least one subcell of the RUC. None of the finite elements has been removed from the analysis, indicating that subcell failure has not been predicted in all material points of the composite layup. The contours of the failed material points agree well with the contours of the Puck matrix criterion.

5 CONCLUSIONS

The analysis in this work shows results of a multiscale methodology application on a numerical model simulating experimental high velocity soft-body impact conditions. Within this two-scale approach, damage effects at the structural level have been determined using micromechanical principles. As explained in Section 2.1, a complex multiaxial damage model, based on a continuum damage mechanics, has been employed to model micro-structural matrix damage. The contours and sizes of the part of the composite plate in which micromechanical degradation effects have been calculated agree very well with results of the Puck failure model. This observation is very promising since Puck's failure model has achieved very good results in the WWFE.

Complete failure of a material point of the FE model has in this work been determined if at least one subcell of the associated unit cell reaches the failure criterion, as explained in Section 2. Validation of micromechanical failure and damage model with WWFE results has been presented in [7]. The results showed that the first subcell failure state for the 30x30 HFGMC model, employed in this work, corresponds to extensive damage evolution throughout the unit cell. Further testing and validation with experimental results are necessary to determine if the selected final failure criterion is physically correct.

This work presents the first results of the micro-structural damage implementation on a macro-structural level, as the methodology is still in development. In the next phase further damage models have to be evaluated. In order to enhance versatility of the methodology, the mesh objective Crack band damage model [15] will be included in the micromechanical damage procedure. The application of micromechanical models for modelling of high velocity impact problems in composite structures is particularly suitable, since such effects in composite materials affect only the matrix. Consequently, viscoplastic effects will be included to matrix constitutive models using the Bodner-Partom model [16].

REFERENCES

[1] Smojver, I. and Ivančević, D. Bird strike damage analysis in aircraft structures using Abaqus/Explicit and Coupled Eulerian Lagrangian approach. *Compos. Sci. Technol.* (2011) **71**: 1725-1797.

[2] Ivančević, D. and Smojver, I. Hybrid approach in bird strike damage prediction on aeronautical composite structures. *Compos. Struct.* (2011) **94**: 15-23.

[3] Aboudi, J., Pindera, M.J. and Arnold, S.M. Higher-order theory for periodic multiphase materials with inelastic phases. *Int. J. Plast*. (2003) **19:** 805-847.

[4] Bansal, Y. and Pindera, M.J. A second look at the Higher-Order Theory for periodic multiphase materials. *J. Appl. Mech.* (2005) **72:** 177-195.

[5] Aboudi, J. Closed form constitutive equations for Metal Matrix Composites. *Int. J. Eng. Sci.* (1987) **25**, 1229-1240.

[6] Bansal, Y. And Pindera, M.J. Finite-Volume Direct Averaging Micromechanics of heterogeneous materials with elastic-plastic phases. *Int. J. Plast.* (2006) **22**: 775-825.

[7] Ivančević, D. and Smojver, I. Micromechanical damage modelling using a two-scale method for laminated composite structures. *Compos. Struct.* (2014) **108**: 223-233.

[8] Bednarcyk, B.A., Aboudi, J. and Arnold, S.M. Micromechanics modeling of composites subjected to multiaxial progressive damage in the constituents. *AIAA Journal* (2010) **48**:

1367-1378.
[9] Haj-Ali, R. and Aboudi, J. Nonlinear micromechanical formulation of the High Fidelity Generalized Method of Cells. *Int. J. Solids Structs.* (2009) **46**: 2577-2592.
[10] Hou, J.P. and Ruiz, C. Soft body impact on laminated composite materials. *Compos. Part A* (2007) **38**: 505-515.
[11] Abaqus Users Manual, Version 6.10-1, Dassault Systémes Simulia Corp., Providence, RI.
[12] Hinton, M.J., Kaddour A.S. and Soden, P.D. A further assessment of the predictive capabilities of current failure theories for composite laminates: comparison with experimental evidence. *Compos. Sci. Technol*. (2004) **64**: 549–588.
[13] Soden, P.D., Hinton, M.J. and Kaddour, A.S. Lamina properties, lay-up configurations and loading conditions for a range of fibre-reinforced composite laminates. *Compos. Sci. Technol.* (1998) **58**: 1011-1022.
[14] Puck, A., Kopp, J. and Knops, M. Guidelines for the determination of the parameters in Puck's action plane strength criterion. *Compos. Sci. Technol*. (2002) **62**: 371 – 378.
[15] Pineda, E.J., Bednarcyk, B.A., Waas, A.M. and Arnold, S.M. Progressive failure of a unidirectional fiber-reinforced composite using the method of cells: Discretization objective computational results. *Int. J. Solids Stuct*. (2013) **50**: 1203-1216.
[16] Goldberg, R.K., Roberts, G.D. and Gilat, A. Incorporation of mean stress effects into the micromechanical analysis of the high strain rate response of polymer matrix composites. *Compos. Part B* (2003) **34**: 151–165.